SPECTROSCOPIC AND STRUCTURAL STUDIES OF DI-UREASILS DOPED WITH LITHIUM PERCHLORATE

S. C. Nunes[a], V. de Zea Bermudez[a*], D. Ostrovskii[b], P. B. Tavares[a], P. C. Barbosa[c], M. M. Silva[c], M. J. Smith[c]

[a] *Departamento de Química and CQ-VR, Universidade de Trás-os-Montes e Alto Douro 5001-801 Vila Real, Portugal*

[b] *Department of Applied Physics, Chalmers University of Technology, 41296 Göteborg, Sweden.*

[c] *Departamento de Química, Universidade do Minho, Gualtar, 4710-057 Braga, Portugal*

Abstract

Di-urea cross-linked POE/siloxane hybrid ormolytes (di-ureasils) doped with a wide concentration range of lithium perchlorate trihydrate ($LiClO_4.3H_2O$) ($200 \geq n \geq 0.5$, where n expresses the salt content in terms of the number of ether oxygen atoms per Li^+ ion) have been analysed by Fourier Transform infrared and Raman (FT-IR and FT-Raman, respectively) spectroscopies and X-ray diffraction (XRD). The results obtained lead us to conclude that the xerogels with $n \geq 5$ are totally amorphous. At $n \leq 1$ free salt is observed. "Free" ClO_4^- ions appear to be the main charge carriers at the conductivity maximum located within the $25 \leq n \leq 8$ composition range of this family of ormolytes. At $n = 15$ ClO_4^- ions coordinated in mono/tridentate (C_{3v} symmetry) and bidentate (C_{2v} symmetry) configurations were detected. In salt-rich samples with $n < 15$ there is a marked tendency for ionic association. The resulting decrease that occurs in the concentration of "free" ions is consistent with the observed significant decrease of the ionic conductivity. The analysis of the "amide I" and

* Tel. +351 259 350 253, Fax: +351 259 350 480, E-mail adress: vbermude@utad.pt

"amide II" regions provided solid proof that the Li^+ ions bond to the urea carbonyl oxygen atoms over the entire range of salt concentration studied.

1. Introduction

Since Wright *et al*. first reported the ionic conduction of complexes formed between linear high molecular weight poly(ethylene oxide) (POE) and alkali metal salts [1], great progress has been achieved in the domain of solid polymer electrolytes (SPEs). These materials have potential application in all-solid-state electrochemical devices, such as high-energy density rechargeable batteries, electrochromic displays (ECDs) and fuel cells [2]. The practical use of the POE-based electrolytes has been somewhat delayed, however, by their poor processability and a marked tendency to crystallise.

In recent years modified SPEs that represent a valuable alternative to conventional polymer electrolytes have been developed using the sol-gel process [3]. This chemical synthetic route provides access to POE/siloxane hybrid networks [4] that offer a number of benefits: (1) a major reduction or even total suppression of crystallinity; (2) good thermal, mechanical and chemical stability; (3) accommodation of high guest salt concentrations without "salting out"; (4) easy processing into thin films. The Li^+-doped ormolyte (organically modified silicate electrolyte) concept has attracted particular interest [5,6,7,8,9,10,11,12,13,14,15].

In this context our group has devoted considerable effort to the investigation of ormolyte systems based on di-urea cross-linked POE/siloxane frameworks (di-ureasils) [16] doped with Li^+ [13,14], Mg^{2+} [17] and Zn^{2+} 18] ions, introduced as triflate salts. Very recently encouraging results were obtained with an ECD prototype incorporating an ormolyte of the di-ureasil family doped with $LiClO_4.3H_2O$ ($200 \geq n \geq 8$) [19]. The di-ureasil host matrix employed, abbreviated as d-U(900) (where d indicates di, U denotes the urea

(-NHC(=O)NH-) group and 900 corresponds to the average molecular weight of the starting organic precursor), comprises POE chains with about 15.5 repeat units. The doped ormolytes have been represented by the notation d-U(900)$_n$LiClO$_4$. Samples with 200 ≥n ≥ 8 are completely amorphous. Thermal degradation starts at 209 ºC in xerogels with n < 25. The highest decomposition temperature (283ºC) was registered at n = 200. The conductivity maximum of this system is located at 15 ≥ n ≥ 8 (approximately 10^{-6} and 10^{-4} Scm^{-1} at 30 and 95 ºC, respectively) [19].

In the present work, d-U(900)$_n$LiClO$_4$ samples with a wider range of salt concentration (200 ≥ n ≥ 0.5) have been examined by FT-IR and FT-Raman spectroscopy with the primary objective of elucidating the Li^+/ether oxygen (POE), Li^+/carbonyl oxygen (urea cross-link) and Li^+/ClO_4^- interactions. The main motivation of this spectroscopic analysis has been to gain insight into the nature/concentration of the species responsible for charge transport. The morphology and structure of the ormolytes studied have been determined by XRD.

2. Experimental Section

2.1. Materials

Lithium perchlorate trihydrate ($LiClO_4.3H_2O$, Aldrich, 99,99%) and O,O'-Bis-(2-aminopropyl) polypropylene glycol-block-polyethylene glycol-block-polypropylene glycol (commercially designated as Jeffamine ED-900®, Fluka, average molecular weight 900 gmol^{-1}) and 3-isocyanatepropyltriethoxysilane (Aldrich 95 %) were used as received. Ethanol (Merck, 99.8%) and tetrahydrofuran (Merck, 99,9%) were dried over molecular sieves prior to use. High purity distilled and deionised water was used in all experiments.

2.2. Synthesis

The synthesis of the $LiClO_4$-doped d-U(900)-based di-ureasils has been described in detail elsewhere [19].

2.3. Experimental techniques

XRD measurements were performed at room temperature with a PW 3040/60 X´Pert Pro Röntgen diffractometer system, using CuK_α radiation (λ = 1.54 Å) and Bragg-Bentano $\theta/2\theta$ geometry. The system includes the ultra-fast X´Celerator detector PW3015/20 and a secondary monochromator. The measurements were performed over the 2θ range of 10-80º. As-prepared and dried xerogel samples were analysed as films (n = 20 and 5) and powders (n = 1, 0.5 and 0). The materials were dried by storage in a dessicator under vacuum at 25 ºC for 20 days.

A Setaram DSC131 Differential Scanning Calorimeter was used to determine the thermal characteristics of the lithium salt. A mass of approximately 10-20 mg was transferred to a 40 µL aluminium can and stored in a dessicator over phosphorous pentoxide under vacuum for two weeks at room temperature. After this drying treatment, the can was hermetically sealed and the thermogram was recorded. The sample was heated from 25 to 300 ºC at 10 ºC min^{-1}. The purge gas used in both experiments was high purity nitrogen supplied at a constant 35 cm^3 min^{-1} flow rate.

The lithium salt sample for thermogravimetric studies was transferred to an open platinum crucible and analysed using a TA Q50 Thermogravimetric Analyser at a heating rate of 10º min^{-1} using dried nitrogen as purge gas (40 mL/min and 60 mL/min in the balance and sample chamber, respectively). Prior to measurement, the sample was vacuum-dried at room temperature for about 48 h.

FT-IR spectra were acquired at room temperature using a Bruker 22 (Vektor) spectrometer placed inside a glove-box with a dry argon atmosphere. The spectra were

collected over the 4000-400 cm^{-1} range by averaging 150 scans at a spectral resolution of 2 cm^{-1}. Solid samples (2 mg) were finely ground, mixed with approximately 175 mg of dried potassium bromide (Merck, spectroscopic grade) and pressed into pellets. Prior to recording the spectra, the pellets were vacuum dried at 80-90 ºC for about 60 h, in order to reduce the levels of adsorbed water and solvent and then transferred into a glove-box.

The FT-Raman spectra were recorded at room temperature with a Bruker IFS-66 spectrometer equipped with a FRA-106 Raman module and a near-infrared YAG laser with wavelength 1064 nm. The spectra were collected over the 3200-300 cm^{-1} range at a resolution of 2 cm^{-1}. The accumulation time for each spectrum was 4 hours.

To evaluate complex FT-Raman band envelopes and to identify underlying spectral components, the iterative least-squares curve-fitting procedure of the PeakFit [20] software package was used throughout this study. The best fit of the experimental data was sought by varying the frequency, bandwidth and intensity of the bands and by employing Voigt band shapes. A linear baseline correction with a tolerance of 0.2% was employed. The standard errors of the curve-fitting procedure were less than 0.002.

3. Results and Discussion

3.1 Structure

The diffractograms of the d-U(900)$_n$LiClO$_4$ di-ureasils reproduced in Fig. 1(a) allow us to conclude that the samples with n = 20 and 5 are amorphous. The characteristic amorphous broad peak, Gaussian in shape and centred at approximately 21.4º in these XRD patterns, is attributed to the coherent diffracting regions of the siliceous network [21]. Structural unit distances of 4.2 and 4.1 Å were obtained for these hybrids, respectively, using the Bragg law. The coherent length L over which the structural unit survives in these two samples was estimated using the modified Scherrer equation $L = I \lambda / (A \cos\theta)$, where A, in radians, is the

integrated area of the peaks and I their intensity. Coherent lengths of 13 and 12 Å were derived for this pair of xerogels, respectively.

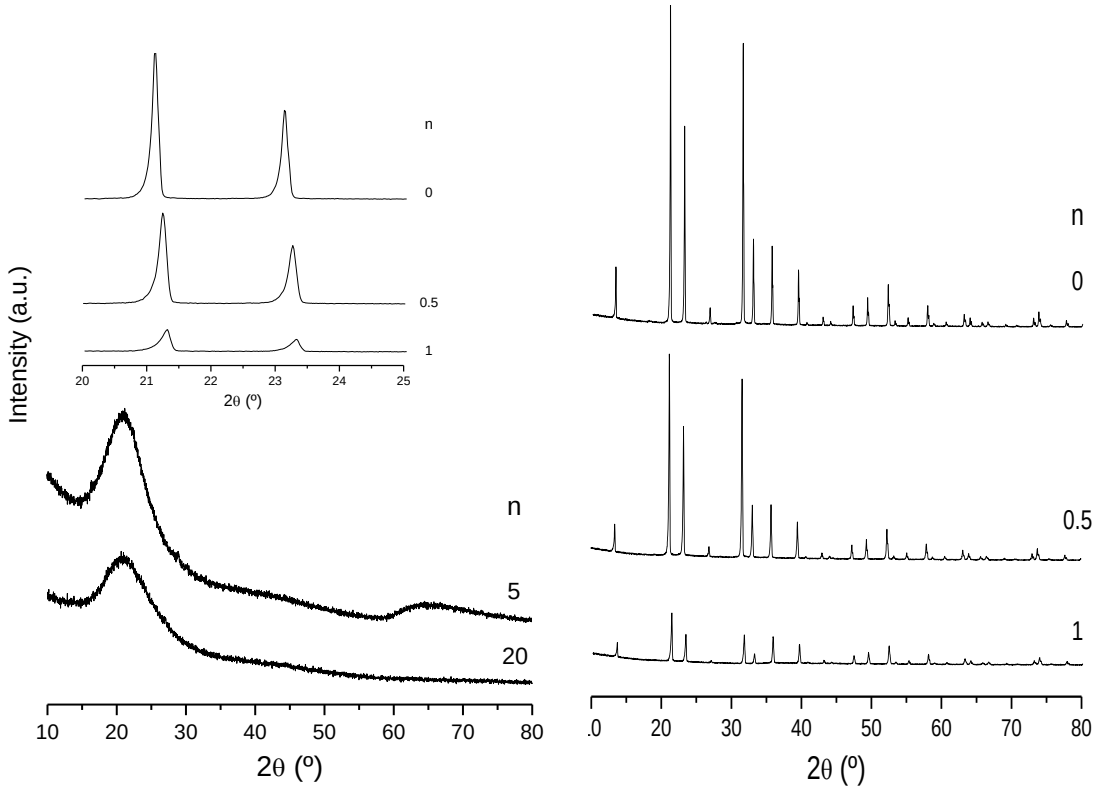

Fig. 1. XRD curves of selected as-prepared d-U(900)$_n$LiClO$_4$ di-ureasils: (a) n ≥ 5 ; (b) n ≤ 1 ; (c) magnification of (b).

In the XRD patterns of the xerogels with n = 1 and 0.5 a series of sharp Bragg reflections, the intensity of which increases as more salt is added, are evident (Fig. 1(b)). Fig. 1(c) reveals that the low angle peaks of these diffractograms and of that of the pure salt are distorted and asymmetrical, demonstrating on the left side a broad shoulder that spreads. A possible explanation for the presence of this asymmetric tail is the existence of intergrowth phenomena between salt with different hydration states (i.e., stacking faults) [22]. A Rietveld refinement of these XRD data (Powder Cell 2.4) [23] indicated that the structure is consistent with a hexagonal cell (P63mc) [24] (Table 1).

Calculated cell parameters are presented in Table 2 for as-prepared and dried samples (see Experimental Section). Upon drying, cell parameters decrease slightly for the pure salt and for the ormolyte with n = 0.5, but increase at n = 1. Crystallite sizes, calculated from Rietveld Powder Cell refinement, range from 120 to 150 nm.

Table 1 - Hexagonal cell parameters for the as-prepared and dried samples

	as-prepared		dried	
n	*a* (nm)	*c* (nm)	*a* (nm)	*c* (nm)
0	7.720	5.449	7.705	5.439
0.5	7.713	5.443	7.709	5.442
1	7.714	5.445	7.725	5.456

The recognition that drying of the ormolyte samples prior to recording the XRD patterns changed the lattice parameters led us to perform DSC and TGA measurements with the guest salt. The DSC curve of the as-received salt shown in Fig. 2 exhibits two endotherms: a sharp, distinct and strong peak with onset at 93 ºC and an ill-defined, multicomponent, broad peak with onset at approximately 125 ºC.

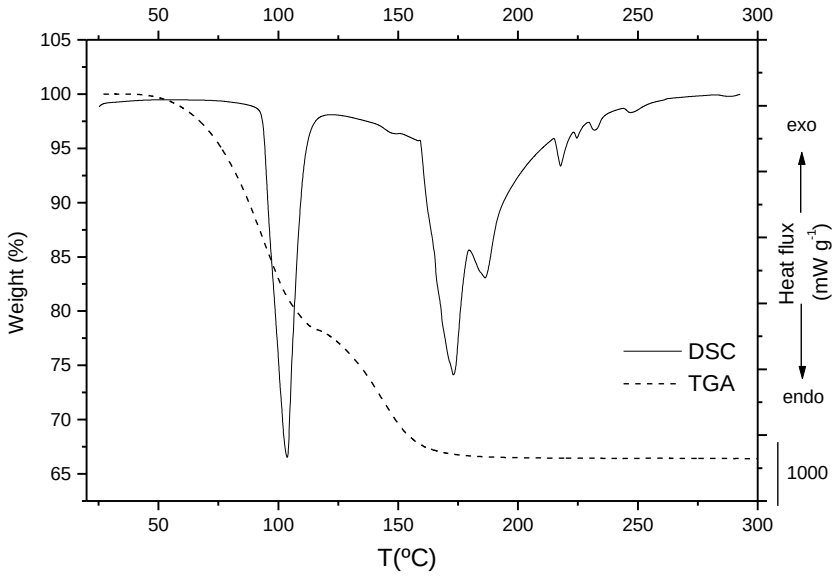

Fig. 2: TGA (left scale) and DSC (right scale) curves of $LiClO_4 \cdot 3H_2O$

Quantitative analysis of the corresponding TGA curve, also seen in the plot of Fig. 2, allowed us to conclude that these events correspond to the loss of two and one water molecules from the cation coordination sphere, respectively, indicating that, after being manipulated in the open atmosphere, the perchlorate salt used in the present work (acquired in the anhydrous state) contains three hydration water molecules. These findings confirm that only drying at sufficiently elevated temperatures yields the anhydrous salt. For instance, we note that the spectroscopic study of Chabanel et al. [25] was carried out using lithium perchlorate dried for 6 h under vacuum and then gently heated it to 300 ºC.

The view of the pure salt structure, deduced from the JMOL software [26] using the data of Table 1, clearly shows that in $LiClO_4.3H_2O$ the Li^+ ions, which line up along the c-axis, are located inside regular hexagonal-shaped channels formed by water molecules (Fig. 3(a)). Fig. 3(a) also allows inferring that the water channels are in turn situated within the voids of hexagonal-like channels composed of ClO_4^- tetrahedra exhibiting an ABAB stacking sequence (planes A solely composed of oxygen atoms and planes B also including Cl^- ions) (Fig. 3(b)).

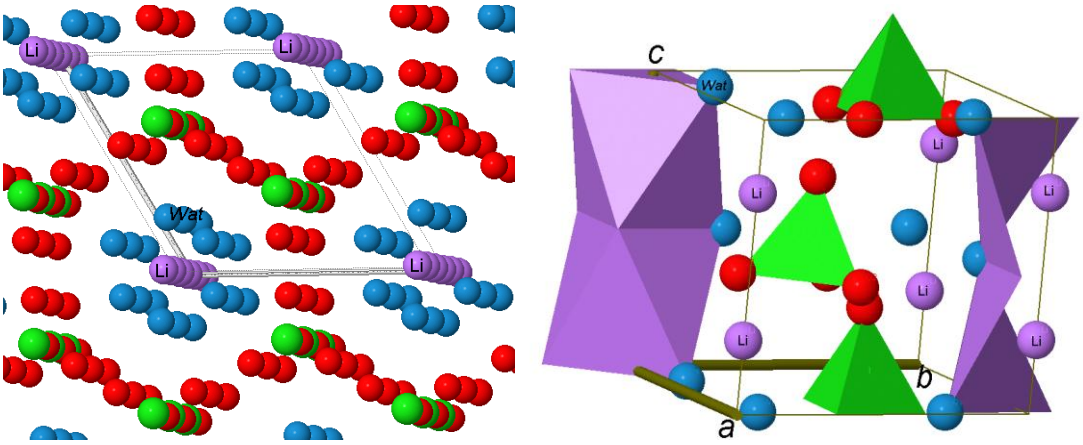

(a) (b)

Fig. 3: Structural model of $LiClO_4.3H_2O$: [001] view of the structure (a) and 3D view of the unit cell (b). Violet spheres - Li^+ ions; green spheres - Cl^- ions; red spheres - perchlorate oxygen atoms and blue spheres - water molecules.

3.2 Cation/anion, cation/POE and cation/cross-links interactions

The charge carrier concentration and ionic mobility are important parameters that influence the conductivity of the electrolyte. Three main types of ionic species can be found in salt/polymer electrolyte systems: (a) “free” or weakly bonded ions with high mobility; (b) cations bonded strongly to the host polymer and with low mobility; (c) ionic aggregates (contact ion pairs and ionic multiplets) with low to moderate mobility. Ionic association in POE/siloxane ormolytes can be investigated using infrared and Raman spectroscopies. Such studies typically involve the use of an ion probe with vibration modes that suffer characteristic changes (e.g., frequency shifts, splitting and/or intensity variations) upon coordination.

The ClO_4^- ion is one of the most widely used anions in the framework of spectroscopic analysis to identify the nature of the ionic species in polymer electrolytes and to determine their concentration [2].

The “free” ClO_4^- ion adopts a tetrahedral (T_d) symmetry and its nine vibrational degrees of freedom are distributed between four normal Raman active modes: $\nu_1(A_1)$, $\nu_2(E)$, $\nu_3(T_2)$ and $\nu_4(T_2)$. Of these, $\nu_1(A_1)$ and $\nu_2(E)$ are inactive in infrared. On the basis of the individual infrared values observed in different solvents, the following average wavenumbers have been deduced for “free” ClO_4^-: $\nu_1(A_1)$ = 931 cm^{-1}, $\nu_3(T_2)$ = 1100 cm^{-1} and $\nu_4(T_2)$ = 624 cm^{-1}. An average wavenumber of 458 cm^{-1} was derived for $\nu_2(E)$ from Raman values [25,27]. The lowering of the local symmetry around ClO_4^- resulting from interaction with a cation leads to band splitting of degenerate vibrations and to frequency shifts of non-degenerate vibrations. In addition, the infrared-forbidden $\nu_1(A_1)$ and $\nu_2(E)$ modes are activated. The magnitude of band separation and frequency shift depends on the strength of ion association. An association of one or three of the ClO_4^- oxygen atoms with a cation (mono- or tridentate coordination,

respectively) lowers the symmetry of the anion to C_{3v}. On the other hand, the association of a cation with two of the ClO_4^- oxygen atoms (bidentate coordination) reduces the symmetry to C_{2v}.

The bidentate configuration of the ClO_4^- ion may be recognised by the splitting of the twofold degenerate ν_2 vibration into two bands (A_1 and A_2) in the Raman spectrum and by the splitting of the threefold degenerate ν_3 and ν_4 vibrations into three components (A_1, B_1 and B_2) both in the infrared and Raman spectra. The mono- or tridentate configurations are manifested through the splitting of the threefold degenerate ν_3 and ν_4 vibrations into two components (A_1 and E) both in the infrared and Raman spectra.

It is accepted that the ClO_4^- symmetry is lowered to C_{3v} when this anion forms contact ion pairs with Li^+ ($Li^{+\cdots}$ ClO_4^-) and to C_{2v} in the so-called dimerized state $Li_2(ClO_4)_2$ [25,27,28].

ν_1ClO_4 region: The FT-Raman non-degenerate symmetric stretching vibration mode of the ClO_4^- ion (ν_1ClO_4) usually shifts to higher wavenumbers [29,30,31,32,33] upon coordination.

The FT-Raman spectra of selected doped d-U(900)-based di-ureasils in the ν_1ClO_4 region and the results of the curve-fitting performed in the ν_1ClO_4 band profiles are represented in Figs. 4(a) and 4(b), respectively. The variation of the integral area fraction of the isolated components with composition is collected in Table 1 and represented in the graph of Fig. 5.

The FT-Raman ν_1ClO_4 band of the d-U(900)$_n$LiClO$_4$ hybrids with $n \geq 15$ was decomposed into three components (Fig. 4(b) and Table 2): a band at 930 cm^{-1} and two shoulders at approximately 925 and 910 cm^{-1}. In the case of d-U(900)$_{15}$LiClO$_4$ a new event emerges at 936 cm^{-1}. In addition, samples with $n \geq 5$ give rise to a very weak feature at about 909 cm^{-1} (Fig. 4(b) and Table 2). The FT-Raman ν_1ClO_4 envelope of the salt-rich sample with n = 1 was resolved into three components at 936, 930 and 925 cm^{-1} (Fig. 4(b) and Table 2).

The 930 cm^{-1} band, observed in all the FT-Raman spectra of the doped samples analysed, is assigned to "free" ClO_4^- ions [25,29,30,31,32,33,34]. The weak event located at 909 cm^{-1} in

the FT-Raman spectra of the Li^+-doped di-ureasils with $n \geq 5$ is associated with the first overtone of the $\nu_2(E)$ deformation mode of the ClO_4^- ion ($2\nu_2ClO_4$) enhanced by Fermi pre-resonance with the ν_1ClO_4 fundamental [25,29,30,31,32]. The 936 cm^{-1} feature probably arises as a result of ion pair formation and is indicative of the presence of ClO_4^- ions coordinated in a monodentate configuration (C_{3v} symmetry) [25,29,30,31,32,33,34]. According to Chabanel et al. [25], the shoulder at 925 cm^{-1} may be correlated with the presence of C_{2v} species. No indication of the formation of dimerised or aggregate species beyond the dimer state have been found in the FT-Raman spectra of the di-ureasils included in this study (at 948 and 961 cm^{-1}, respectively [25]).

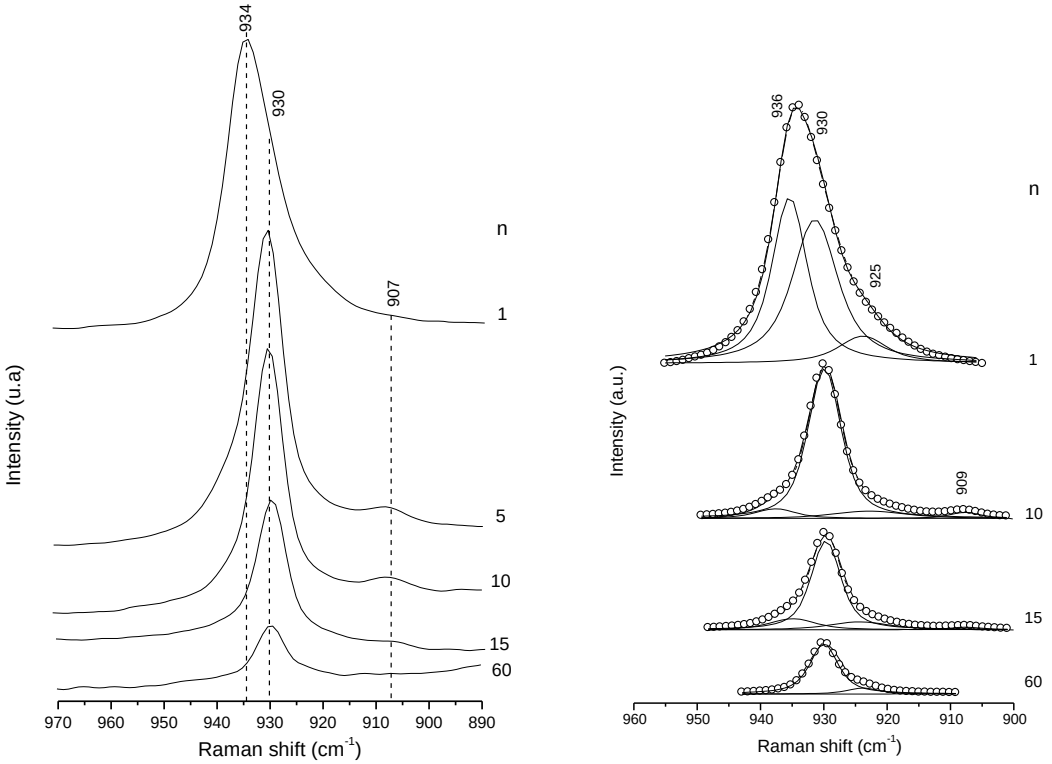

Fig. 4: FT-Raman spectra of selected d-U(900)$_n$LiClO$_4$ di-ureasils in the ν_1ClO_4 region (a) and curve-fitting results of representative samples (b). The frequencies indicated represent the average value of the frequencies of all the samples considered.

The graph included in Fig. 5 demonstrates that the relative intensity of the three ν_1ClO_4 components remains practically unchanged in xerogels with $60 \geq n \geq 5$. Upon further addition

of salt (n = 1) the concentration of monodentate ClO_4^- ions increases significantly at the expense of a reduction of the "free" anions (Fig. 5).

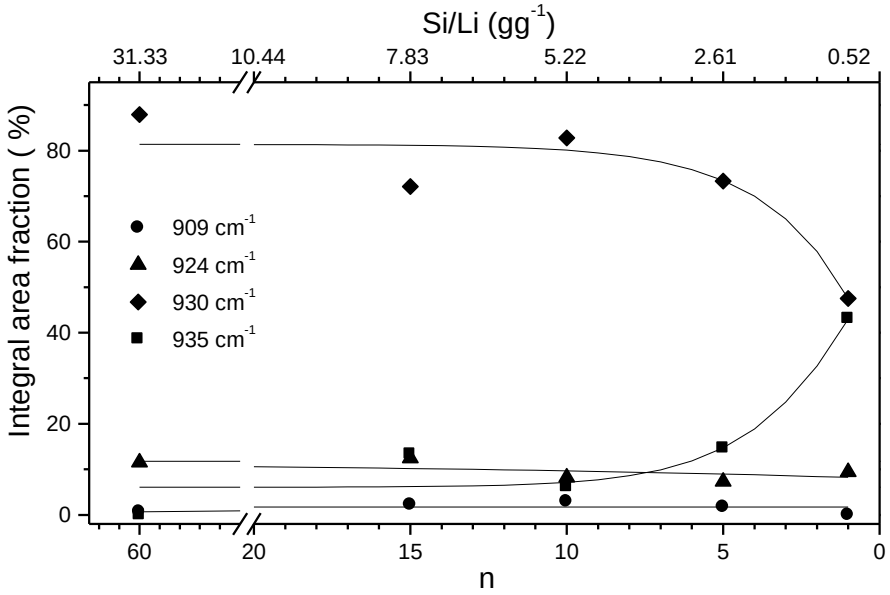

Fig. 5: Composition dependence of the integral area fraction of the isolated components of the FT-Raman ν_1ClO_4 band of the d-U(900)$_n$LiClO$_4$ di-ureasils.

Table 2 – Composition dependence of the integral area fraction (%) of the resolved components (cm^{-1}) of d-U(900)$_n$LiClO$_4$ di-ureasils in the FT-Raman ν_1ClO_4, ν_2ClO_4 and ν_4ClO_4 regions.

ClO_4^-	**n**										**Attribution**	**Ref.**
	60		15		10		5		1			
mode	ν	Area	ν	Area	ν	Area	ν	Area	ν	Area	configuration ClO_4^-	
	-	-	935	13.3	936	6.2	935	14.7	935	43.1	monodentate ($Li^+ClO_4^-$)	25,29-34
ν_1	930	87.9	930	72.1	930	82.7	930	73.3	931	47.5	"free"	25,29-34
	924	11.5	925	12.4	923	8.2	923	7.3	925	9.4	bidentate	25
	912	0.66	909	2.2	909	2.9	909	1.7			$2\nu_2ClO_4$	25,29-33
	-	-	-	-	-	-	-	-	639	18.4	bidentate	25
ν_4			630	2.8	630	6.6	628	21.0	632	40.9	bidentate	25
			623	97.2	623	93.4	623	79.0	623	40.7	free	25
					463	26.3	465	18.5	463	53.3	bidentate	25,38
ν_2					457	60.8	458	54.7	460	37.7	"free"	35-37
					451	12.9	454	26.7	454	9.8	bidentate	25,38

ν_2ClO_4 region: The FT-Raman spectra of the doped di-ureasil materials in the region characteristic of the doubly degenerate deformation mode of the ClO_4^- ion (ν_2ClO_4) are reproduced in Fig. 6(a). The results of the curve-fitting performed on the ν_2ClO_4 band of selected samples are depicted in Fig. 6(b). The variation of the integral area fraction of the isolated components with composition is collected in Table 2.

The FT-Raman ν_2ClO_4 band of the doped d-U(900)-based hybrids with n = 10 and 5 was decomposed into three components (Fig. 6(b) and Table 2): a band at 459 cm^{-1} and two weak shoulders at 465 and 453 cm^{-1}. The FT-Raman ν_2ClO_4 envelope of the di-ureasil with n = 1 was also resolved into the same three components (Fig. 6(b). and Table 2). However, in the latter case the 465 cm^{-1} event dominates this spectral region, followed by the band at 460 cm^{-1} and finally by the feature at 453 cm^{-1} (Fig. 6(b) and Table 2).

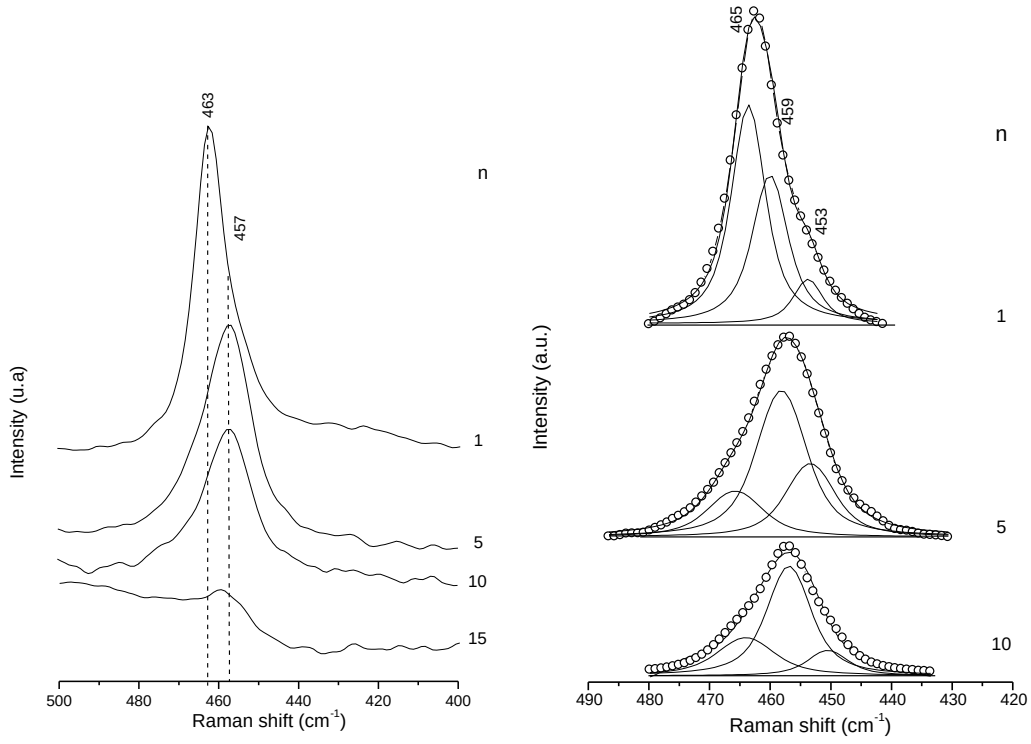

Fig. 6: FT-Raman spectra of selected d-U(900)$_n$LiClO$_4$ di-ureasils in the ν_2ClO_4 region (a) and curve-fitting results of representative samples (b). The frequencies indicated represent the average value of the frequencies of all the samples considered.

The 459 cm^{-1} band is assigned to "free" ClO_4^- ions [35,36,37]. The existence of the two additional bands strongly supports the occurrence of C_{2v} symmetry and thus bidentate contact association between Li^+ and ClO_4^- [25,38]. Within the C_{2v} symmetry the 465 and 453 cm^{-1} components are attributed to $\nu_2(A_1)$ and $\nu_2(A_2)$ modes, respectively [25,38].

ν_3ClO_4 and νCOC regions: In the FT-IR spectra of the d-U(900)$_n$LiClO$_4$ samples the triply degenerate asymmetric stretching mode of the ClO_4^- ion (ν_3ClO_4) is superimposed on the polymer skeleton COC stretching (νCOC) mode (Fig. 7).

The FT-IR spectrum of d-U(900) exhibits a strong band around 1110 cm^{-1} and a shoulder at about 1145 cm^{-1} (Fig. 7) [39]. These events are attributed to the νCOC vibration mode and to the coupled vibration of the νCOC and rCH_2 modes, respectively, and are characteristic of non-complexed, amorphous polyether chains [40,41,42]. As the intensity and frequency of both features persists essentially unchanged in samples with $n \geq 20$, we are led to conclude that in this salt composition interval the ether oxygen atoms of the polymer segments do not participate in the coordination of the Li^+ ions and that the POE chains remain amorphous. With the increase of salt concentration (n = 5) four bands emerge (Fig. 7): two intense, sharp features at 1122 cm^{-1} (very strong) and 1108 cm^{-1} (strong) and two ill-defined, broad bands at 1144 cm^{-1} and 1090 cm^{-1} (unresolved multiplet). Fig. 7 demonstrates that the further addition of salt (n = 1) leads to a marked growth of the 1144, 1108 and 1092 cm^{-1} events.

The lifting of the triply degeneracy of the ν_3ClO_4 mode into three components provides evidence that the local environment of ClO_4^- must be at least C_{2v} [27]. The spacing between the most separated components of the ν_3ClO_4 region (1144 - 1092 = 52 cm^{-1}) is identical to that found in solid alkaline metal perchlorates [25], but considerably lower than that reported for argon matrices (226 cm^{-1}) [43]. The 1122 cm^{-1} feature may be tentatively ascribed to the

presence of coordinated ClO_4^- ions in a C_{3v} configuration [25]. The 1144, 1122 and 1108 cm^{-1} envelopes are characteristic of the $\nu_3(T_2)$ vibration of the pure crystalline salt [25].

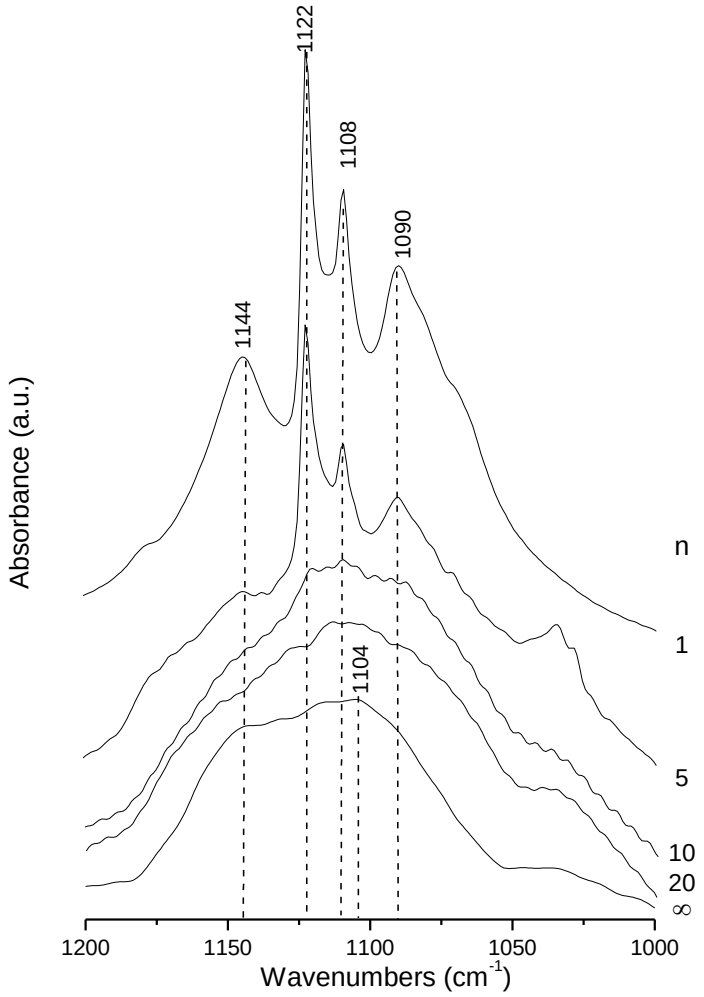

Fig. 7: FT-IR spectra of selected d-U(900)$_n$LiClO4 di-ureasils in the □ν_3ClO_4 and νCOC regions. The frequencies indicated represent the average value of the frequencies of all the samples considered.

ν_4ClO_4 region*:* The FT-IR and FT-Raman spectra of selected d-U(900)$_n$$LiClO_4$ di-ureasils in the region characteristic of the triply-degenerate deformation vibration mode of the ClO_4^- ion (ν_4ClO_4) are reproduced in Figs. 8(a) and 9(a), respectively. The results of the curve-fitting carried out in the FT-IR and FT-Raman ν_4ClO_4 bands for representative xerogels are

given in Figs 8(b) and 9(b), respectively. The variation of the integral area fraction of the FT-Raman/FT-IR isolated components with composition is collected in Table 2 and Fig. 10/ Table 3.

The FT-IR ν_4ClO_4 mode of the d-U(900)$_n$LiClO$_4$ hybrid with n = 10 was decomposed into five components at 637, 633, 630, 626 and 622 cm^{-1} (Fig. 8(b) and Table 2). In the samples with n = 5 and 1 two new components develop at 640 and 619 cm^{-1} respectively (Fig. 8(b) and Table 2).

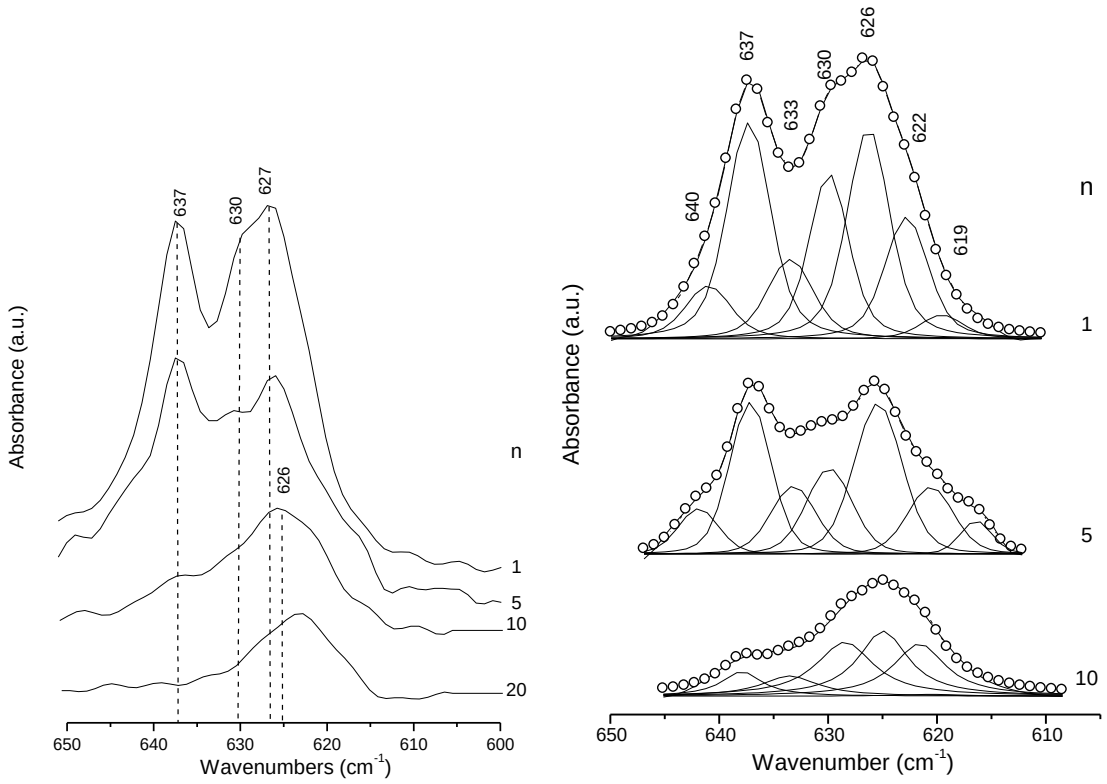

Fig. 8: FT-IR spectra of selected d-U(900)$_n$LiClO$_4$ di-ureasils in the ν_4ClO_4 region (a) and curve-fitting results of representative samples (b). The frequencies indicated represent the average value of the frequencies of all the samples considered.

The FT-Raman ν_4ClO_4 envelope of the Li^+-based d-U(900) doped hybrids with n = 15, 10 and 5 was resolved into only two components: one band at 623 cm^{-1} and a shoulder at 630

cm^{-1} (Fig. 9(b) and Table 2). Upon further addition of salt (n = 1), this shoulder becomes the strongest ν_4ClO_4 component and a new event appears at 639 cm^{-1} (Fig. 9(b) and Table 2). The presence of three components in the FT-Raman ν_4ClO_4 envelope of the d-U(900)$_1$LiClO$_4$ compound supports the explanation that the local symmetry around ClO_4^- is C_{2v} [25]. These findings lead us to propose that the FT-Raman feature seen at 623 cm^{-1} is simultaneously associated with "free" and bidentate coordinated ClO_4^- ions [25].

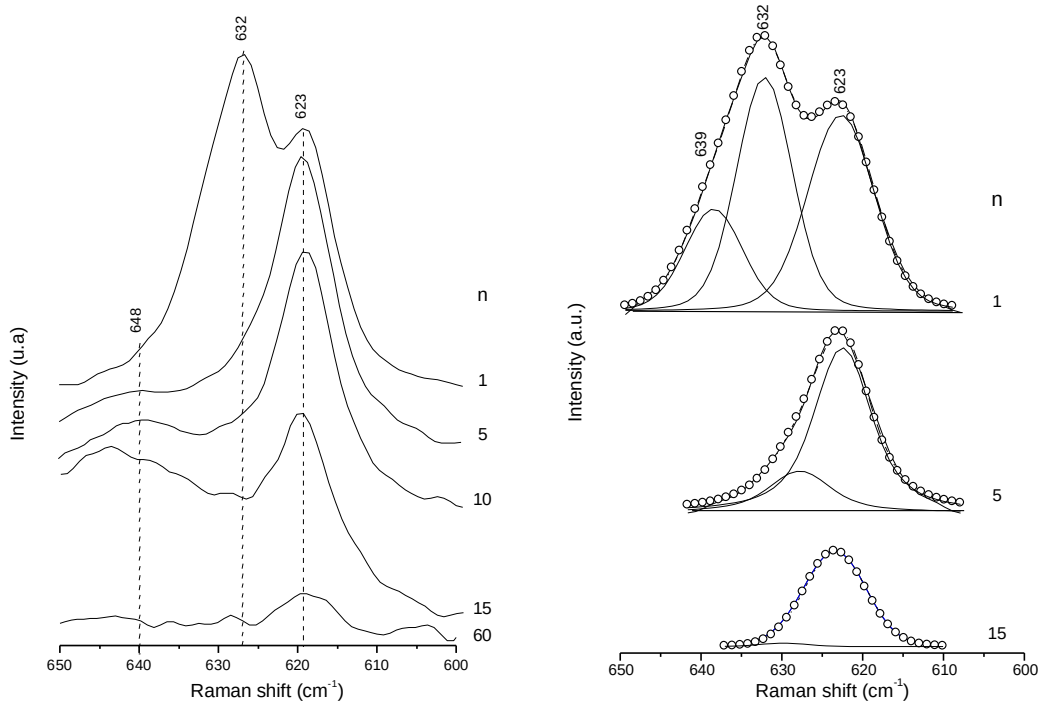

Fig. 9*:* FT-Raman spectra of selected d-U(900)$_n$LiClO$_4$ di-ureasils in the ν_4ClO_4 region (a) and curve-fitting results of representative samples (b). The frequencies indicated represent the average value of the frequencies of all the samples considered.

The 633, 626 and 622 cm^{-1} bands observed in the FT-IR ν_4ClO_4 region (Fig. 8(b) and Table 3) are attributed to ClO_4^- ions in a bidentate configuration, suggesting that the local symmetry around ClO_4^- must be C_{2v} [25]. We note that the FT-IR feature seen at 626 cm^{-1} appears to be common to "free" and bidentate coordinated ClO_4^- ions. The FT-IR events at

630 and 619 cm^{-1} (Fig. 8(b) and Table 3) correspond to $^{37}ClO_4$ isotopomers [25]. It is very likely that the feature at 637 cm^{-1} and the shoulder at 640 cm^{-1} are associated with monodentate bonded ClO_4^- ions [25,32].

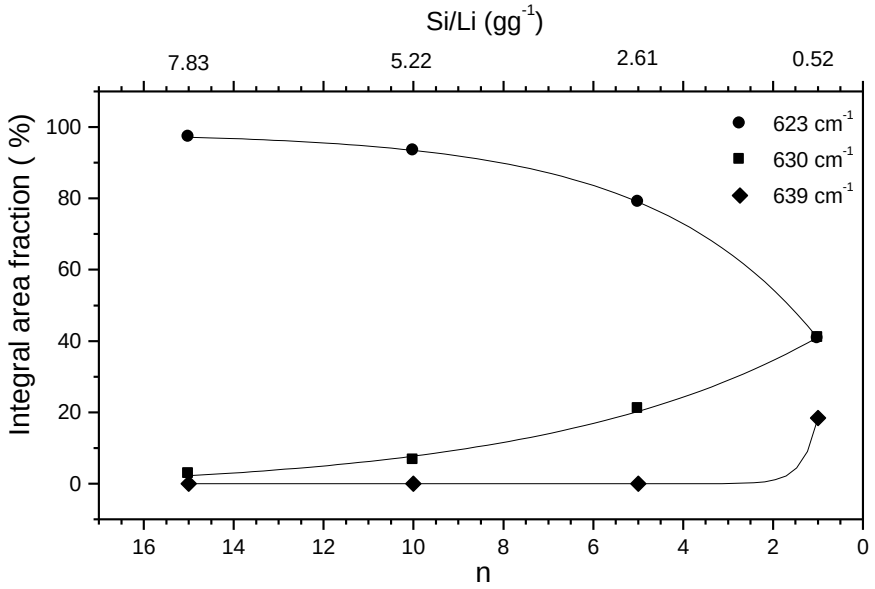

Fig. 10: Composition dependence of the integral area fraction of the isolated components of the FT-Raman ν_4ClO_4 band of the d-U(900)$_n$LiClO$_4$ di-ureasils.

Fig. 10 reveals that the relative intensity of the three ν_4ClO_4 components remains essentially unaltered in samples with n = 15 and 10. The incorporation of more salt (n = 5) leads to a moderate increase of the proportion of bidentate ClO_4^- ions (Fig. 10). A reduction of the fraction of "free" ions occurs in parallel (Fig. 10). At n = 1 the concentration of "free" ions markedly decreases and the proportion of bidentate ClO_4^- ions continues to grow (Fig. 10). As expected, the trend exhibited by the "free" ν_4ClO_4 component as a function of composition is in perfect agreement with that displayed by the corresponding ν_1ClO_4 feature (cf. Fig. 5). The spectroscopic analysis performed in the present work has enabled us to

conclude that in the salt-rich d-U(900)$_n$LiClO$_4$ samples with n ≤ 5 there is clearly a marked tendency for ionic association.

Table 3 – Composition dependence of the integral area fraction (%) of the resolved components (cm^{-1}) of the more concentrated d-U(900)$_n$LiClO$_4$ di-ureasils in the FT-IR ν_4ClO$_4$ region.

n						***Atribution***	***Ref.***
10		**5**		**1**			
ν	Area	ν	Area	ν	Area		
		642	6.8	640	6.4	monodentate ClO_4^- ($Li^+ClO_4^-$)	25
637	8.5	637	23.7	637	25.3	monodentate ClO_4^- ($Li^+ClO_4^-$)	25,32
633	9.9	633	11.7	633	9.9	bidentate ClO_4^-	25
628	27.3	630	14.9	630	17.6	isotopic $^{37}ClO_4^-$	25
625	29.1	626	27.4	626	24.0	"free" and bidentate ClO_4^-	25
622	24.1	621	11.6	623	14.1	bidentate ClO_4^-	25
-	-	617	3.9	620	2.7	isotopic $^{37}ClO_4^-$	25

This observation is consistent with the significant decrease of the ionic conductivity observed at n < 8 [19]. However, we would like to emphasize that the interpretation proposed should be treated with caution, since although the frequencies of the perchlorate bands in the FT-IR and FT-Raman spectra of the hybrid materials studied here exactly match those reported for the same anion in solutions of LiClO$_4$ in several aprotic donor solvents [27], the species responsible for the bands found in the di-ureasils may be considerably different. Only by measuring the transference numbers, a study that is beyond the scope of the present work, could we confirm the claim that the "free" ClO_4^- species are the main charge carriers in samples with compositions in the vicinity of the conductivity maximum.

"Amide I and amide II" regions: In this section the examination of the FT-IR spectra of the d-U(900)$_n$LiClO$_4$ hybrids in the "amide I" (1800-1600 cm^{-1}) and "amide II" (1600-1500 cm^{-1}) regions, reproduced in Fig. 11 was carried out with the objective of determining the ranges of salt concentration in which the carbonyl oxygen atoms of the urea cross-links bond

to the Li^+ ions. This analysis will enable us to obtain in parallel valuable information regarding the extent of hydrogen bonding in these xerogels.

The "amide I" region of the di-ureasils corresponds to the amide I [44] region of polyamides [45]. The amide I mode is a complex vibration that receives a major contribution from the C=O stretching vibration and is sensitive to the specificity and magnitude of hydrogen bonding. [45] Usually the amide I band consists of several components which correspond to different C=O environments known as aggregates, associations or structures. As the absorption coefficients of C=O groups belonging to these aggregates can be different, it is not possible to compare intensity values of different components. Consequently, only the changes suffered by each mode represent concentration variations of each aggregate [45,46].

The "amide II" mode of the di-ureasils corresponds to the amide II [44] mode of polyamides [45]. The amide II band is a mixed mode that contains a major contribution from the N-H in-plane bending vibration [44]. As it is sensitive to both chain conformation and intermolecular hydrogen bonding, this mode gives reliable information about the distribution of hydrogen bond strengths [44].

The analysis of Fig. 11 demonstrates that the addition of Li^+ ions to d-U(900) host matrix affects the "amide I" and "amide II" regions of all the di-ureasils examined, an indication that the Li^+ ions interact with the carbonyl oxygen atoms of the urea cross-links over the entire concentration range considered. It may be immediately inferred from Fig. 11 that the "amide I" region of the di-ureasils is extremely complex.

Curve-fitting of the "amide I" mode of the d-U(900) matrix (not shown) permitted the identification of the strong components around 1678 and 1646 cm^{-1} and the two shoulders located at about 1756 and 1723 cm^{-1}. The band at 1756 cm^{-1} is associated with the absorption of urea groups in which the N-H or C=O groups are free from any interactions [47]. The bands centred near 1723 and 1678 cm^{-1} are ascribed to the absorption of hydrogen-bonded

C=O groups of disordered hydrogen-bonded POE/urea associations of increasing strength [47]. Finally, the 1646 cm^{-1} feature is assigned to the absorption of C=O groups included in significantly more ordered hydrogen-bonded urea/urea associations [47]. The band at 1565 cm^{-1} is ascribed to the "amide II" mode (Fig. 11).

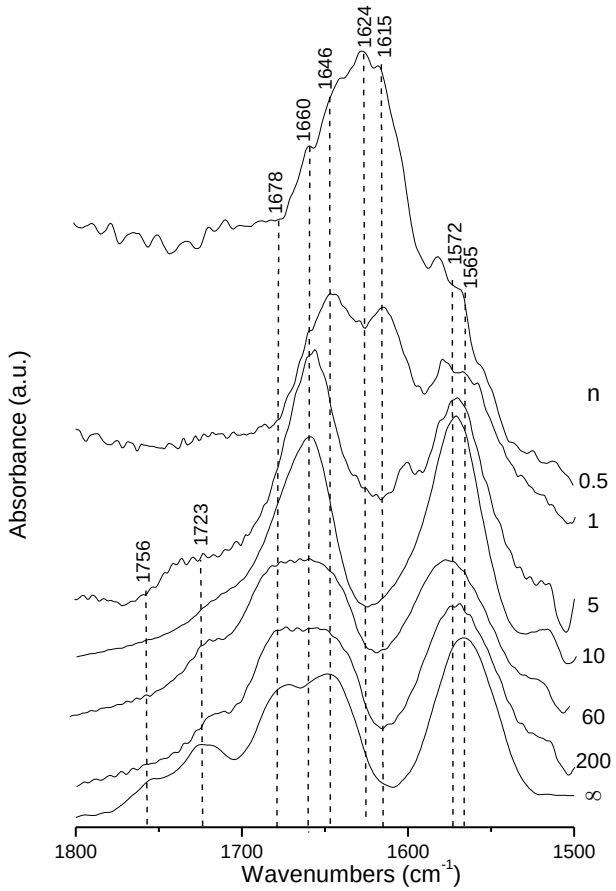

Fig. 11: FT-IR spectra of selected d-U(900)$_n$LiClO$_4$ di-ureasils in the "amide I" and "amide II" regions. The frequencies indicated represent the average value of the frequencies of all the samples considered.

The analysis of Fig. 11 demonstrates that the addition of Li^+ cations to the d-U(900) host matrix perturbs the "amide I" region, solid evidence that the alkali metal ions coordinate to the carbonyl oxygen atoms of the urea cross-links over the whole range of salt concentration examined. The two intense broad bands of the "amide I" envelope of d-U(900), situated

around 1678 and 1646 cm^{-1}, due to ordered POE/urea structures, are replaced by a single broad band centred at 1660 cm^{-1} in samples with n =10 and 5 (Fig. 11). The 1756 and 1723 cm^{-1} features practically disappear upon salt addition. At n = 1 saturation of the urea cross-links is attained. In addition, at this composition, the band at 1660 cm^{-1} becomes a shoulder and a band at 1646 cm^{-1}, attributed to urea/urea aggregates, is transformed into a more intense event. At n = 0.5 the intensity maximum is located at 1624 cm^{-1} and a new event emerges at 1624 cm^{-1} (Fig. 11). These findings suggest that the hydrogen-bonded associations formed at high salt content are more ordered (and thus stronger) than those found in the less concentrated hybrids.

The intense "amide II" mode of the d-U(900) observed at 1565 cm^{-1} (Fig. 11) shifts to 1572 cm^{-1} upon addition of salt, a clear indication that the hydrogen bonds established are stronger than those observed in the host matrix. In salt-rich materials with n = 1 and 0.5 the "amide I" and "amide II" bands are superimposed (Fig. 11).

4. Conclusions

Di-ureasil ormolytes doped with a wide concentration of $LiClO_4.3H_2O$ ($200 \leq n \leq 05$) were prepared by the sol-gel method and analysed by FT-IR and FT-Raman spectroscopy and XRD.

Structural data revealed that free salt exists in samples with n = 1 and 0.5. The hydration state of the guest salt is a critical parameter to consider in the characterisation of the samples.

Xerogels with high to moderate ionic conductivity are amorphous. "Free" ClO_4^- ions appear to be the main charge carriers of the conductivity maximum of this family of ormolytes located within the $25 \leq n \leq 8$ composition range. At n = 15 ClO_4^- ions coordinated through mono-/tri- and bidentate configurations (C_{3v} and C_{2v} symmetry, respectively) appear. In the salt-rich samples with n < 15 the marked tendency for ionic association that occurs at

the expense of a drastic reduction in the concentration of "free" ions is consistent with a significant decrease of the ionic conductivity.

The analysis of the "amide I" and "amide II" regions provided solid proof that the Li^+ ions bond to the urea carbonyl oxygen atoms over the entire range of salt concentration studied.

Acknowledgments

The authors are pleased to acknowledge the support provided by Universidade do Minho and Universidade de Trás-os-Montes e Alto Douro and Fundação para a Ciência e a Tecnologia (contracts POCI/QUI/59856/2004, POCTI/SFA/3/686 and SFRH/BD/2207/2005).

List of figure captions

Fig. 1. XRD curves of selected d-U(900)$_n$$LiClO_4$ di-ureasils.

Fig. 2: TGA (left) and DSC (right) curves of $LiClO_4.3H_2O$

Fig. 3: Structural model of $LiClO_4.3H_2O$: [001] view of the structure (a) and 3D view of the unit cell (b). Violet spheres - Li^+ ions; green spheres - Cl^- ions; red spheres - perchlorate oxygen atoms and blue spheres - water molecules.

Fig. 4. FT-Raman spectra of selected d-U(900)$_n$$LiClO_4$ di-ureasils in the ν_1ClO_4 region (a) and curve-fitting results of representative samples (b). The frequencies indicated represent the average value of the frequencies of all the samples considered.

Fig. 5: Composition dependence of the integral area fraction of the isolated components of the FT-Raman ν_1ClO_4 band of the d-U(900)$_n$$LiClO_4$ di-ureasils.

Fig. 6: FT-Raman spectra of selected d-U(900)$_n$LiClO$_4$ di-ureasils in the ν_2ClO_4 region (a) and curve-fitting results of representative samples (b). The frequencies indicated represent the average value of the frequencies of all the samples considered.

Fig. 7: FT-IR spectra of selected d-U(900)$_n$LiClO$_4$ di-ureasils in the ν_3ClO_4 and νCOC regions.

Fig. 8: FT-IR spectra of selected d-U(900)$_n$LiClO$_4$ di-ureasils in the ν_4ClO_4 region (a) and curve-fitting results of representative samples (b). The frequencies indicated represent the average value of the frequencies of all the samples considered.

Fig. 9: FT-Raman spectra of selected d-U(900)$_n$LiClO$_4$ di-ureasils in the ν_4ClO_4 region (a) and curve-fitting results of representative samples (b). The frequencies indicated represent the average value of the frequencies of all the samples considered.

Fig. 10: Composition dependence of the integral area fraction of the isolated components of the FT-Raman ν_4ClO_4 band of the d-U(900)$_n$LiClO$_4$ di-ureasils.

Fig. 11: FT-IR spectra of selected d-U(900)$_n$LiClO$_4$ di-ureasils in the "amide I" and "amide II" regions. The frequencies indicated represent the average value of the frequencies of all the samples considered.

Tables

Table 1 – Hexagonal cell parameters for the as-prepared and 20 days vacuum dried samples

Table 2 - Composition dependence of the integral area fraction (%) of the resolved components (cm^{-1}) of d-U(900)$_n$LiClO$_4$ di-ureasils in the FT-Raman ν_1ClO_4, ν_2ClO_4 and ν_4ClO_4 region.

Table 3 - Composition dependence of the integral area fraction (%) of the resolved components (cm^{-1}) of the more concentrated d-U(900)$_n$LiClO$_4$ di-ureasils in the FT-IR ν_4ClO_4 region.

References

[1] B. E. Fenton, J. M. Parker, P. V. Wright, Polym.14, (1973) 589.

[2] F. M. Gray, Polymer Electrolytes, RSC Materials Monographs, Royal Society of Chemistry, London, (1997)

[3] C. J. Brinker, G. W. Scherer, Sol-Gel Science: The Physics and Chemistry of Sol-Gel Processing, Academic Press, San Diego, CA, (1990)

[4] P. Gomez-Romero, C. Sanchez (Eds), Functional Hybrid Materials, Wiley Interscience, New York, (2003)

[5] D. Ravaine, A. Seminel, Y. Charbouillot, M. Vincens, J. Non-Cryst. Solids, 82, 210 (1986)

[6] M. Popall, M. Andrei, J. Kappel, J. Kron, K. Olma, B. Olsowski, Electrochim. Acta, 43 (10-11) (1998) 1155

[7] P. Judeinstein, J. Titman, M. Stamm, H. Schmidt, Chem. Mater., 6, 127 (1994)

[8] K. Dahmouche, M. Atik, N. C. Mello, T. J. Bonagamba, H. Panepucci, M. A. Aegerter, P. Judeinstein, J. Sol-Gel Sci. Technol., 8, 711 (1997)

[9] V. de Zea Bermudez, L. Alcácer, J. L. Acosta, E. Morales, Solid State Ionics, 116, 197 (1999)

[10] C. Wang, Y. Wei, G. R. Ferment, W. Li, T. Li, Mater. Lett., 39, 206 (1999)

[11] J. R. MacCallum and S. Seth, Eur. Polym. J., 36, 2337 (2000)

[12] K. Nishio and T. Tsuchiya, Sol. Energy Mater. Sol. Cells, 68, 295 (2001)

[13] S. C. Nunes, V. de Zea Bermudez, D. OstrovskiI, M. M. Silva, S. Barros, M. J. Smith, R. A. Sá Ferreira, L. D. Carlos, J. Rocha, E. Morales, J. Electrochem. Soc., 152(2) (2005) A429

[14] S. C. Nunes, V. de Zea Bermudez, M. M. Silva, M. J. Smith, L. D. Carlos, R. A. Sá Ferreira, J. Rocha, J. Solid State Electrochem., 10(4) (2006) 203.

[15] C. Sanchez, B. Julián, P. Belleville, M. Popall, J. Mater. Chem., 15 (2005) 3559

[16] M. Armand, C. Poinsignon, J.-Y. Sanchez and V. de Zea Bermudez, U.S. Patent 5, 283, 310, 1993

[17] S. C. Nunes, V. de Zea Bermudez, M. M. Silva, S. Barros, M. J. Smith, E. Morales, L. D. Carlos, J. Rocha, Solid State Ionics, 176/17 (2005) 1591-1599

[18] S. C. Nunes, V. de Zea Bermudez, M. M. Silva, M. J. Smith, E. Morales, R. A. Sá Ferreira, L. D. Carlos, J. Rocha, Solid State Sciences, in press

[19] P. C. Barbosa, M. M. Silva, M. J. Smith, A. Gonçalves, E. Fortunato, Electrochim. Acta, in press

[20] PeakFit is a product of Jandel Corporation, 2591 Rerner Boulevard, San Rafael, CA 94901, U.S.A. 8

[21] L. D. Carlos, V. de Zea Bermudez, R. A. Sá Ferreira, L. Marques, M. Assunção, Chem. Mater. 11(3) (1999) 581

[22] J. Cmaidalka , A. Baikalov , Y. Y. Xue , R. L. Meng and C. W. Chu, Physica C: Superconductivity, 403(3) (2004) 125.

[23] W. Kraus, G. Nolze, PowderCell for Windows, version 2.3, available at http://ccp14.minerals.csiro.au/ccp/web-mirrors/powdcell/a_v/v_1/powder/e_cell.html

[24] A. Sequeira, I. Berrad, I. D. Brow, R. Faggiari, Acta Cryst. B 31 (1975) 1735

[25] M. Chabanel, D. Legoff, K. Touaj, J. Chem. Soc., Faraday Trans., 92(21) (1996) 4199

[26] JMOL software available at Inorganic Crystal Structure Database (ICSD for WWW), URL http://icsd.ill.fr

[27] S. Ross, Spectrochim. Acta 18 (1962) 225.

[28] L. Ducasse, M. Dussauze, J. Grodin, J.-C. Lassegues, C. Naudir, L. Servant, Phys. Chem. Chem. Phys. 5 (2003) 567.

[29] J. R. Stevens, P. Jacobsson, Can. J. Chem. 69 (1991) 1980; 737.

[30] J. Grodin, L. Ducasse, J. L. Bruneel, L. Servant, J. C. Lassegues, Solid State Ionics, 166 (2004) 441.

[31] X. Huang, T. Ren, L. Tian, L. Hong, W. Zhun, X. Tang, J. Mater. Sci. 39 (2004) 1221.

[32] M. Marcinek, M. Ciosek, G. Zukowska, W. Wieczorek, K. R. Jeffrey, Solid State Ionics 176 (2005) 367.

[33] M. H. Brooker, A. S. Quist, G. E. Boyd, Chem. Phys. Lett., 9 (3) (1971).

[34] M. M. Silva, S. C. Nunes, P. C. Barbosa, A. Evans, V. de Zea Bermudez, M. J. Smith, D. Ostrovskii, Electrochim. Acta (2006) (in press).

[35] R. Frech, J. P. Manning, Electrochim. Acta 37 (9) (1992) 1499.

[36] S. Schantz, L. M. R Torell, J. R. Stevens, J. Appl. Phys. 64 (1988) 2038.

[37] M. Kakihana, S. Schantz, L. M. Torell, L. Borjesson, Mat. Res. Soc. Symp. Proc. 135 (1989) 107.

[38] A. G. Miller, J. W.Macklin, J. Phys Chem 89 (1985) 1193.

[39] V.de Zea Bermudez, L. D. Carlos, L. Alcácer, Chem. Mater. 11 (1999) 569

[40] K. Machida, T. Miyazawa, Spectrochim. Acta 20 (1964), p. 1865

[41] H. Matsuura, T. Miyazawa, J. Polym. Sci. 7(A-2) (1969), p. 1735

[42] V. Di Noto, D. Longo, V. Münchow, J. Phys. Chem. B, 103 (1999), p. 2636

[43] G. Rizthaupt, J. P. Devlin, J. Chem. Phys. 62 (1976) 1982.

[44] T. Miyazawa, T. Shimanouchi, S.-I. Mizushima, J. Chem. Phys. 24(2) (1956) 408.

[45] D. J. Skrovanek, S. E.Howe, P. C. Painter, M. M. Coleman, Macromolecules 18 (1985) 1676.-

[46] M. M. Coleman, K. H. Lee, D. J. Skrovanek, P. C. Painter, Macromolecules, 1986, 19, 2149

[47] V. de Zea Bermudez, L. Alcácer, L. D. Carlos, Chem. Mater. 11 (1999) 569